JOURNAL OF COMPUTATIONAL PHYSICS 93, 449–468 (1991)

FLAIR: Flux Line-Segment Model for Advection and Interface Reconstruction

N. ASHGRIZ AND J. Y. POO

Department of Mechanical and Aerospace Engineering, State University of New York at Buffalo, Buffalo, New York 14260

Received February 21, 1989; revised January 9, 1990

A computational technique for solving fluid problems with free surfaces and interfaces is presented. The conventional cell volume fraction approach is employed for tracking the interfaces. However, for surface advection and its reconstruction, a new and more accurate FLAIR (flux line-segment model for advection and interface reconstruction) algorithm is developed. The surface is approximated by a set of line segments fitted at the boundary of every two neighboring computational cells. A criterion is developed for identifying the line-segment orientation by inspecting the cell volume fractions. The new cell volume fraction field is obtained by integrating the advected area underneath the interface linesegment. As an example, this technique is applied to the capillary driven viscous flow of an initially elliptic, two-dimensional fluid zone. The problem is posed mathematically as a solution of the Navier–Stokes equations with moving free surface boundary conditions. The damping motion of the fluid zone is observed through transport of the free surface, which is related to the instantaneous internal velocity field under the influence of surface tension and viscous forces.

INTRODUCTION

Analytical treatment of free surfaces and interfaces is an issue of major importance in many of the fundamental and practical fluid mechanic problems. The mathematical description of fluid interface transport involves the solution of the governing equations of motion on the fluid domain, part of which includes interfaces. The exact locations of these interfaces are not known a priori and must be determined as part of the solution of the transport equations. Numerical description of free surface flows and interfaces is notoriously complicated due to the difficulties associated with the discrete representation of the interfaces, their temporal evolution and spatial convolution, and the manner in which the boundary conditions are imposed.

There are variety of numerical methods for treating fluid problems with interfaces. The most common one is the boundary-integral technique [1–3]. However, this technique is currently restricted to the limiting cases of either zero Reynolds number, or inviscid irrotational flows. Other methods, available for handling free-surface flow problems are the finite-element methods [4–6], the methods using

0021-9991/91 $3.00

581/93/2-14

boundary-fitted orthogonal coordinates [7–9], and Lagrangian methods [10, 11]. At present, these techniques cannot handle surface foldings and surface merging and their application to very deformed surfaces has yet to be demonstrated.

A totally different category of numerical techniques which have the potential for handling large surface deformations and surface folding and merging is that of volume tracking methods. These methods use a volumetric progress variable, such as marker particles in the marker and cell (MAC) technique [12–15], and the cell volume fraction in the volume of fluid (VOF) technique [16–19], for Lagrangian transport of the interfaces. The marker and cell method involves Eulerian flow-field calculations and Lagrangian liquid–particle movements. The velocity of a marker is found by taking the average of the Eulerian velocities in its vicinity. One difficulty in using the MAC method is the possible creation of artificially high or low marker number densities in the cells, due to the irregularity of the flow field.

The volume of fluid (VOF) method is much easier to use and less computationally intensive. Two major problems arise when the interface is represented by a fractional volume parameter. One is how to identify the exact surface location and the other is how to advect the surface. Several techniques have been introduced for moving the volume fraction field. A common one is the so-called donor–acceptor technique [19–21]. This technique is based on describing a surface orientation and then moving the surface with the velocity normal to that orientation. In the donor–acceptor technique, the surface cell is assumed to be either horizontal or vertical. The decision regarding the orientation is made based on studying the neighboring cells. Once the surface orientation is identified, different techniques can be used for its advection [22–24]. The donor–acceptor technique, which is used in the VOF method, emphasizes control of interface diffusion rather than control of the liquid fraction in a cell. Therefore, ad hoc techniques must be designed to remove "bad" points. For example, cells having liquid fractions either less than zero or greater than unity are corrected by redistributing liquid around them.

Other techniques have also been reported [25, 26], which have improved the accuracy of the surface reconstruction and its advection in VOF based codes. For instance DeBar [25], and Youngs [26] have used sloped line segments in each cell rather than horizontal and vertical ones as was discussed for the donor–acceptor method. The interface slope in each cell is obtained by inspecting the volume fractions of the neighboring cells. The slope of a line that will cut through two or three neighbor cells and will result in the correct cell volume fractions is obtained. The sloped interface is then convected by the local velocities at the cell. Unfortunately DeBar [25] and Youngs [26] have not reported the details of their techniques for calculating the surface slopes. Therefore, no further discussion on their methods can be given here.

Clearly, the accuracy of the techniques that use sloped line segments to represent the interface is crucially dependent on the method of calculating the slope of this line segment. In this paper we describe a technique which represents the fluid interface by a set of sloped line segments which are fitted at the boundary of every two neighboring cells. A rigorous technique is developed for finding the slope of the line

segment and the advection of the interface. The method is demonstrated by considering several free surface problems.

FLAIR Algorithm

Consider an Eulerian square mesh system, as shown in Fig. 1, and an actual curved surface cutting through it. Lets assume that this curve is the free surface of a liquid below it in a 2D flow field. Therefore, one can define an area (or volume) fraction parameter, f, that can take values between 1 and 0. That is $f=0$ represents an empty cell, $f=1$ a full cell, and $0<f<1$ a surface cell. We will call a cell with $f>0$ a " wet cell." We propose to solve the following problem. Given the f field and the velocity components u and v in x and y directions, respectively, first, what is the surface shape and its curvature and, second, how does the surface move. In our previous paper on this topic [27], we proposed a second-order accurate technique for calculating surface curvature, given the f field. Here we are introducing a new algorithm for the calculations of advection and reconstruction of surfaces.

An interface can be viewed as composed of line segmens if the grid system is fine enough. Locally this line segment can be forced at the cell boundary by examining the area fractions of the two adjacent cells. The distinct feature of this method is to find the slope of this line segment based only on two neighboring volume fractions. Figure 2 is presented to amplify the differences between FLAIR and conventional line segment approaches. In conventional line segment approaches the actual surface (Fig. 2a) is represented by a set of horizontal and vertical lines. For instance in SLIC method by Noh [5] the surface is reoriented in a manner shown in Figs. 2b and c. Where, all the surfaces are considered to be vertical for flux calculations in the x-direction and horizontal for flux calculations in the y-direction. In VOF method by Nichols *et al.* [4] the surface orientation is also considered to be either vertical or horizontal (Fig. 2d), except that in their algorithm the decision

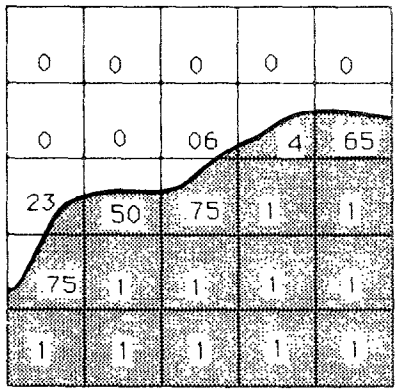

Fig 1. A typical volume fraction field.

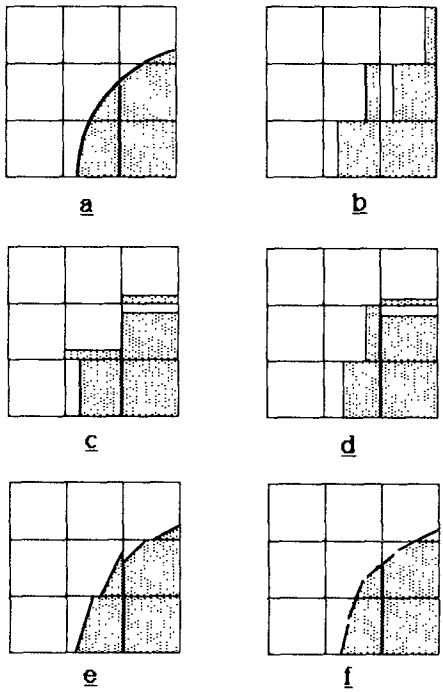

FIG. 2. Comparisons of different interface representation techniques.

on the type of surface orientation is made according to a weighting criterion based on the cell's neighboring volume fractions. In Youngs' [26] method the line-segment has a slope (Fig. 2e), but it is fitted inside each cell. Therefore, the flux calculations in their method will resemble the previous techniques with slight improvement in accuracy. In the FLAIR technique the line segments are drawn at the cell boundaries as shown in Fig. 2f. When moving the interface, the fluid underneath the trapezoid generated by each line segment is moved with the velocity given at the cell boundary. We will show that this technique will result in a more accurate interface advection.

By examining the fractional area in each cell pair at the surface, one of the conditions shown in Fig. 3 can be identified. For instance, if we define the volume fraction in the cell on the left as f_a, and that on the right f_b, case one corresponds to $0 < f_a < 1$, and $f_b = 0$, case two corresponds to $f_a = 0$ and $0 < f_b < 1$, and case nine corresponds to $0 < f_a < 1$ and $0 < f_b < 1$. However, the exact surface orientation or the slope of the surface line is yet to be determined based on the given area fractions in the two cells. The technique presented below is designed to generate a unique description of the surface slope. The method for finding the surface slope for case 9 is discussed first. It is then shown that all of the other cases can be reduced to this case.

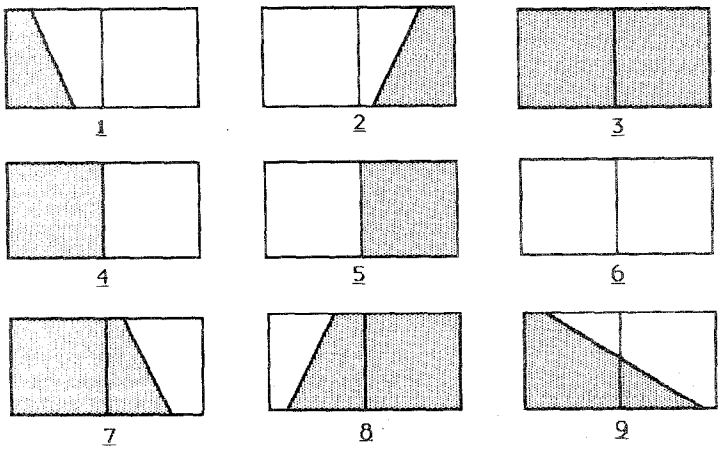

FIG. 3. Existing relations for two neighboring cells.

In order to be able to identify the surface orientation in case 9, one can identify four possible conditions by inspection. These four subcases of case 9 are shown in Fig. 4. Figure 4a shows the interface line connecting the left sidewall to the right sidewall; Fig. 4b shows the left sidewall to the bottom wall; Fig. 4c shows the top wall to right sidewall; and Fig. 4d the top wall to the bottom wall. The method for determining the surface line is given below.

Subcase (a). Two neighboring cells can always be reoriented such that $f_a \geqslant f_b$. The interface is assumed to be a simple line segment fitted through the boundary of two neighboring cells. Therefore, the interface can be represented by

$$y = ax + b, \tag{1}$$

where constants a and b are to be determined based on the known area fractions f_a and f_b. Therefore, the area underneath the line will be

$$\int_{x_1}^{x_2} y\,dx = \tfrac{1}{2}a(x_2^2 - x_1^2) + b(x_2 - x_1). \tag{2}$$

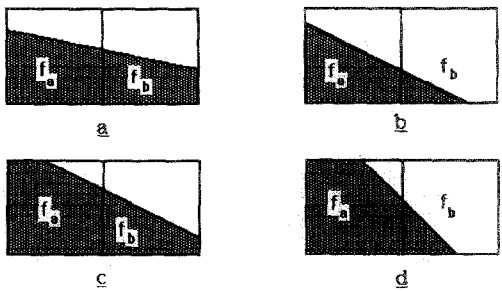

FIG. 4. Possible interfacial structures for case 9.

If the cell size is $h \times h$, then

$$f_a h^2 = \tfrac{1}{2} a h^2 + bh$$
$$f_b h^2 = \tfrac{3}{2} a h^2 + bh.$$

Solving for a and b,

$$a = f_b - f_a \tag{3}$$

$$b^* = \frac{b}{h} = \frac{1}{2}(3f_a - f_b). \tag{4}$$

Once the surface is reconstructed, the fluid flux moving from one cell to the other cell can be calculated as follows: Defining $s = u\,\delta t/h$, where u is the fluid velocity at the boundary of the two cells and δt is the time step in the calculations, the flux of fluid in the positive x direction (δf^+) will be (see Fig. 5)

$$\delta f^+ = s[a + b^* - as/2] \tag{5}$$

and the flux in the negative x direction (i.e., if u is negative) is

$$\delta f^- = s[a + b^* + as/2]. \tag{6}$$

Subcase (b). The equations to be considered for this subcase are

$$0 = a x_b^* + b^*$$
$$f_a = a/2 + b^*$$
$$f_b = (a/2)(x_b^{*2} - 1) + b^*(x_b^* - 1),$$

where $x_b^* = x_b/h$ and x_b is the point of intersection of the line segment and the cell bottom. This results in the following solutions for a and b^*:

$$a = 2(f_a - b^*) \tag{7}$$

$$b^* = 2[(f_a + f_b) - \sqrt{f_a f_b + f_b^2}]. \tag{8}$$

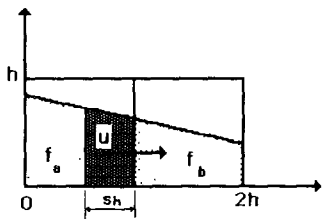

FIG. 5. Liquid flux calculation method for two neighboring interfacial cells.

The corresponding fluid fluxes are

$$\delta f^+ = s[a + b^* - as/2] \tag{9}$$

$$\delta f^- = \begin{cases} f_b & \text{if} \quad s+1 \geqslant x_b^* \\ s(a+b^*+as/2) & \text{if} \quad s+1 < x_b^*. \end{cases} \tag{10}$$

Subcase (c). Similarly,

$$a = 2(2f_a + f_b - 3 + 2\sqrt{(1-f_a)(2-f_a-f_b)}) \tag{11}$$

$$b^* = 3(3 - 2f_a - \tfrac{2}{3}f_b - 2\sqrt{(1-f_a)(2-f_a-f_b)}) \tag{12}$$

and

$$\delta f^+ = \begin{cases} s(a+b^*-as/2), & \text{if} \quad s \leqslant 1 - x_a^* \\ s + f_a - 1, & \text{if} \quad s > 1 - x_a^* \end{cases} \tag{13}$$

$$\delta f^- = s(a + b^* + as/2), \tag{14}$$

where $x_a^* = x_a/h$, and x_a is the interception point at the top cell boundary.

Subcase (d).

$$a = 1/(x_a^* - x_b^*) \tag{15}$$

$$b^* = x_b^*/(x_a^* - x_b^*). \tag{16}$$

Here the normalized points of intersection (x_a^* and x_b^*) are

$$x_a^* = 1 - \frac{2(1-f_a)}{l}$$

$$x_b^* = 1 + \frac{2f_b}{(1-l)},$$

where

$$l = 1 \Big/ \left(\sqrt{\frac{f_b}{1-f_a}} + 1 \right)$$

$$\delta f^+ = \begin{cases} s(a+b^*-as/2), & \text{if} \quad s \leqslant 1 - x_a^* \\ s + f_a - 1 & \text{if} \quad s > 1 - x_a^* \end{cases} \tag{17}$$

$$\delta f^- = \begin{cases} f_b & \text{if} \quad s+1 \geqslant x_b^* \\ s(a+b^*+as/2) & \text{if} \quad s+1 < x_b^* \end{cases} \tag{18}$$

Surface Identification

Once we have developed a set of equations for each of the four different interface subcases shown in Fig. 4, we are ready to set up a criterion for determining the

interface type by only inspecting the area fraction fields. That is, knowing f_a and f_b, it is desired to determine the case that represents the surface orientation. For instance, the criterion for case one is given as follows. Based on Eqs. (1), (3), and (4), the equation for the surface line of Subcase (a) is

$$y=(f_b-f_a)x+\frac{h}{2}(3f_a-f_b).$$

We can see from Fig. 4a that

$$h\geqslant y(0)=\frac{h}{2}(3f_a-f_b)\geqslant 0.$$

Therefore,

$$2\geqslant(3f_a-f_b) \tag{a}$$

and

$$3f_a-f_b\geqslant 0. \tag{b}$$

We can also write

$$h\geqslant y(2h)=(f_b-f_a)2h+\frac{h}{2}(3f_a-f_b).$$

This results in the following inequalities:

$$2\geqslant 3f_b-f_a \tag{c}$$

and

$$3f_b-f_a\geqslant 0. \tag{d}$$

Noting that (a) is more restrictive than (c), based on our initial assignment of $f_a\geqslant f_b$, the following equations can be obtained for f_a and f_b of Subcase (a):

$$\begin{aligned} 3f_b&\geqslant f_a\\ 2&\geqslant 3f_a-f_b. \end{aligned} \tag{19}$$

The same type of analysis can be carried out for all the other subcases. The final results are

Subcase (b).

$$\begin{aligned} 3f_b&\leqslant f_a\\ f_a+f_b-\sqrt{f_af_b+f_b^2}&\leqslant 0.5. \end{aligned} \tag{20}$$

Subcase (c).

$$\begin{aligned} f_a+f_b+\sqrt{(1-f_a)(2-f_a-f_b)}&\geqslant 1.5\\ f_a+f_b/3+\sqrt{(1-f_a)(2-f_a-f_b)}&\leqslant \tfrac{4}{3}. \end{aligned} \tag{21}$$

Subcase (d).

$$f_a - \sqrt{f_b(1-f_a)} \geq 0.5$$
$$f_b(1+\sqrt{(1-f_a)/f_b}) \geq 0.5. \tag{22}$$

Based on the above criteria a case distinction diagram can be constructed which will identify different cases based on only f_a and f_b. Figure 6 shows that such a diagram for case 9 as a function of f_a and f_b. Different regions in this figure are defined as follows:

Curve OD:

$$f_b + \sqrt{f_b(1-f_a)} = 0.5.$$

Curve OA:

$$3f_a - f_b = 2.$$

Curve OB:

$$f_a - 3f_b = 0.$$

Curve OC:

$$f_a - \sqrt{f_b(1-f_a)} = 0.5.$$

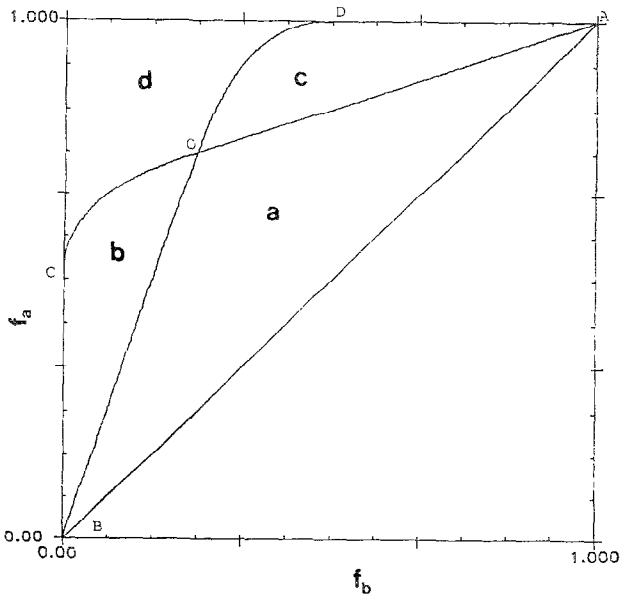

FIG. 6. Case distinction diagram for case 9.

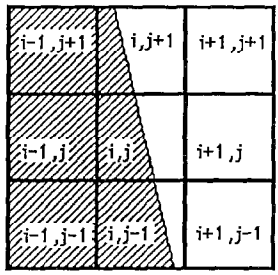

FIG. 7. An interfacial representation for case 1.

For a wet cell moving into a dry cell, such as in cases 1 and 2, the line segment must be found within the cell rather than at the cell boundary. The slope of this line segment is found by taking the average of the slopes found at the cell boundaries between the wet cell and its neighboring wet cells. Consider the 3×3 cell unit shown in Fig. 7. The cell pair (i, j) and $(i+1, j)$ represent case 1, where $0 < f_a = f_{i,j} < 1$, and $f_b = f_{i+1,j} = 0$.

The slope of the line segment in cell (i, j) can be calculated by averaging the two slopes obtained with the same technique as described for case 9, by once using $f_{i,j-1}$ and $f_{i,j}$ and the other time using $f_{i,j}$ and $f_{i,j+1}$ (e.g., the volume fractions of two neighboring cells to cell (i, j) in the vertical direction). Once the slope of the line segment is calculated the following criterion is developed to identify the type of the wet cell. By inspection four different subcases for a single wet cell (as shown in Fig. 8) are identified. Knowing the surface slope, β, and the value of volume fraction, f_a, a surface-type distinction diagram is developed to identify the surface type. This diagram, which is a plot of f_a versus β, is shown in Fig. 9. For a pair of f_a and β, only one of the four types of line segments in Fig. 8 can be identified. In Fig. 9 the curves which separate different regions are as follows: OA is $f_a = 1 - 1/(2\beta)$; OB is $f_a = 1/(2\beta)$; OC is $f_a = \beta/2$; and OD is $f_a = 1 - \beta/2$. Upon

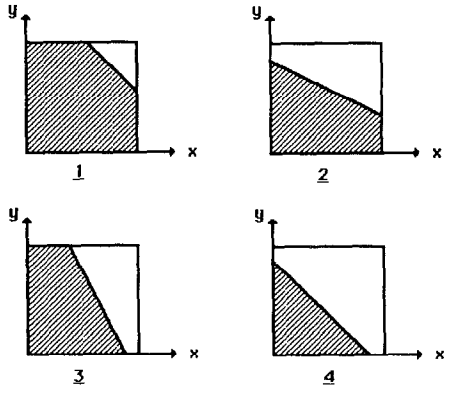

FIG. 8. Possible interfacial line-segment in a cell.

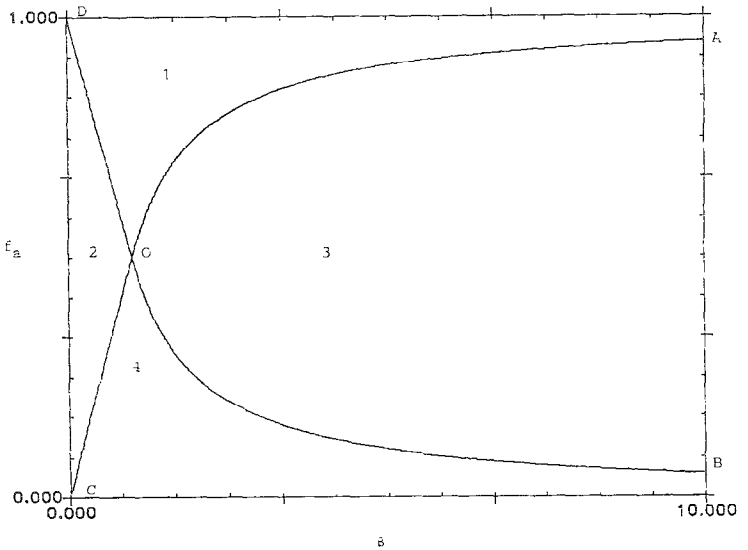

FIG. 9. Case distinction diagram for the line-segment in an interfacial cell.

knowing the type of line segment in a cell a fluid flux calculation can be carried out. The fluid flux calculation is the integration of the area covered by the line segment when it is moved with the velocity component at the cell boundary.

In cases 3, 4, and 5, cells are either full or empty and therefore the surface orientation is known. Cases 7 and 8 are similar to cases 1 and 2, and again the neighboring wet cells have to be inspected to obtain the surface orientation. By simple inspection it can be seen that the surface orientation for all the cases are either already known or they can be reduced to case 9.

An algorithm can then be constructed to identify each case. Once the interface orientation is identified, it can be moved in Lagrangian sense with local velocities at the cell boundaries with the following procedure. In the x-sweep every two horizontally adjacent cells are considered. Based on f_a and f_b, one of the cases in Fig. 3 is identified. Then, depending on the case chosen, the particular movement procedure is used. The fluid fluxes in the x-direction are all calculated based on x-direction velocity component, u. A new f field is generated based on the calculated fluid fluxes. The new f field is then used in the y-sweep, and this time fluid fluxes in the y-direction are calculated based on the y-direction velocity component, v. In order to determine u and v at the cell boundaries momentum equations are solved. This is described in the next section.

ADVECTION AND RECONSTRUCTION OF A CIRCLE

FLAIR is tested and compared with the more common donor–acceptor method. The first test is concerned with movement of a circle. In Fig. 10 the fluid movement

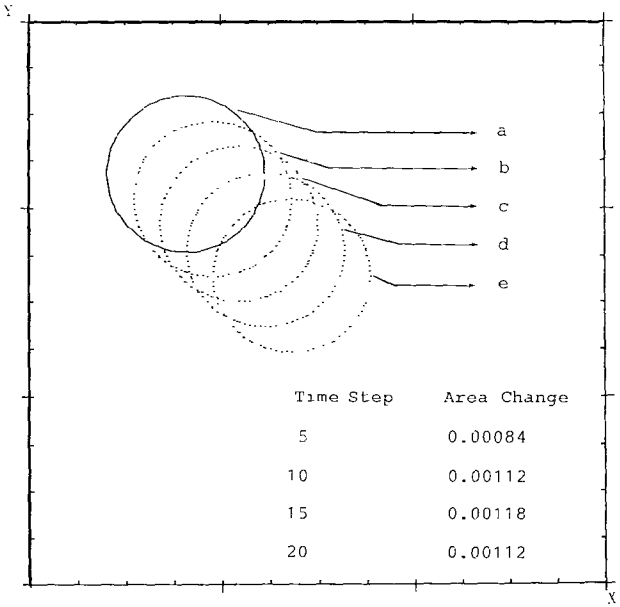

FIG. 10. A circular region moved across the computational domain.

method is tested by moving a circular fluid region across the computational meshed domain. The test conditions are as follows. A uniform velocity field is given to the circular region, which is initially at the upper-left position. Given the size of the circle initially, a cell area fraction field is computed. FLAIR technique is then applied to the area fraction field with a time step just enough to move the fluid half a grid size to the right and half a grid size downward. The circular region is moved in this way for 20 time steps until the circle is moved out of its original position. The area fraction field thus obtained is then examined to see the error that is accumulated during the movement. From Fig. 10, which is obtained by plotting the point where the line segment intercepts the cell boundary, it is quite clear that the circle is moved with very good accuracy. The resultant error in the area change is also shown in Fig. 10. The area change is defined as the original circle area minus the area at any other time. The area at any time is calculated by adding all the area fractions. This is a good indicator of the accuracy of the method used for the interface advection.

In order to demonstrate the difference between FLAIR method and the donor–acceptor method, a small segment of a circle is advected using both techniques. Figure 11a shows the initial volume fractions of a small segment of a circle. Figure 11b shows the results obtained using FLAIR method after two time steps, and Fig. 11c shows the results from the donor–acceptor method at the same two time steps. The accuracy of FLAIR over donor–acceptor method is clearly shown by a one-to-one comparison of the volume fractions at the end of the calculation.

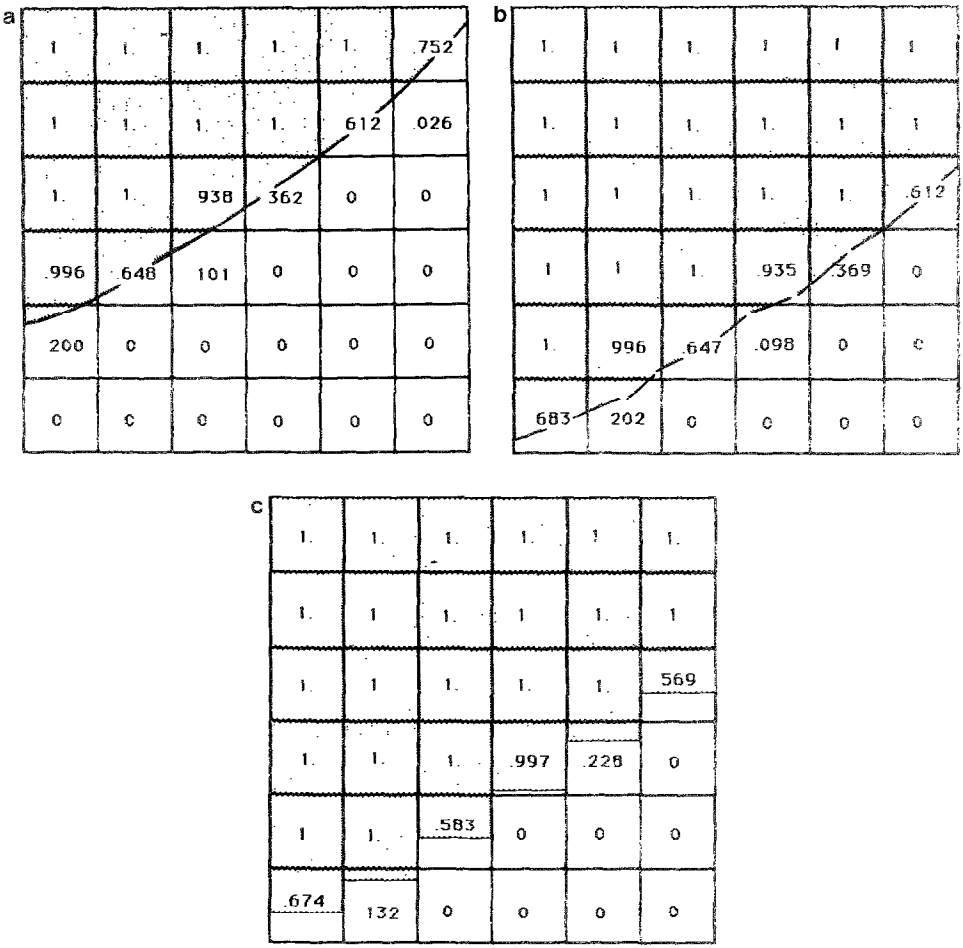

FIG. 11. Comparison of volume fraction field advection Technique between donor–acceptor and FLAIR methods: (a) original volume fraction field; (b) the new field using FLAIR; and (c) the new field using donor–acceptor.

The donor–acceptor movement results in the loss of second surface layer. For instance, the initial volume fractions in the first and second layer of the third column are 0.938 and 0.101, respectively. When the surface is advected using donor–acceptor method, the new volume fractions of 0.997 and 0.00 are obtained. A better prediction of 0.935 and 0.098 is resulted by using the FLAIR method.

CAPILLARY-DRIVEN DROP MOTION

A two-dimensional elliptic fluid region is chosen to present the technique for handling the free surface boundary conditions in the momentum equation and also

to test the accuracy of the technique. The initially elliptic fluid zone is described using a square mesh system. The surface of the ellipse crosses through the mesh system and generates fractional volume parameters in each of the boundary cells. The fractional areas are therefore initially assigned. The fractional areas for all the interior cells are set equal to one, and those for the exterior cells are set equal to zero. The following equations are solved for the capillary-driven viscous flow of the region described above.

Governing Equations of Motion

The two-dimensional, incompressible, constant properties Navier–Stokes equations with free boundaries are solved. For this problem, the continuity, momentum, and Poisson's equations are:

$$\frac{\partial u}{\partial x}+\frac{\partial v}{\partial y}=0 \tag{23}$$

$$\frac{\partial u}{\partial t}+\frac{\partial uu}{\partial x}+\frac{\partial uv}{\partial y}=-\frac{\partial p}{\partial x}+\frac{1}{\mathrm{Re}}\left(\frac{\partial^2 u}{\partial x^2}+\frac{\partial^2 u}{\partial y^2}\right) \tag{24}$$

$$\frac{\partial v}{\partial t}+\frac{\partial vu}{\partial x}+\frac{\partial vv}{\partial y}=-\frac{\partial p}{\partial y}+\frac{1}{\mathrm{Re}}\left(\frac{\partial^2 v}{\partial x^2}+\frac{\partial^2 v}{\partial y^2}\right) \tag{25}$$

$$\frac{\partial^2 p}{\partial x^2}+\frac{\partial^2 p}{\partial y^2}=2\left(\frac{\partial u}{\partial x}\frac{\partial v}{\partial y}-\frac{\partial u}{\partial y}\frac{\partial v}{\partial x}\right). \tag{26}$$

Boundary Conditions

At the present time we are only considering the motion of a fluid zone in vacuum. Therefore, no shear forces are present at the fluid surface. Also, the effect of velocity gradients on the surface pressure is neglected. Hence, the boundary equation simply becomes

$$p=\frac{\sigma}{R}=\frac{-\sigma y_{xx}}{(1+y_x^2)^{1.5}}, \tag{27}$$

where R is the curvature at the surface and σ is the surface tension.

Method of Solution

The equations of motion are solved using a fully implicit scheme having staggered grids. However, special care has to be taken in writing the finite difference equations for the surface cells. Based on inspection of all possible conditions at the surface, five situations can be identified. These five cases are shown in Fig. 12. Note that there is only one situation that wil result in case 1; four situations for case 2; four for case 3; four for case 4; and four for case 5.

At the free surface, the momentum equation cannot be evaluated the same way it is in the interior of the fluid because the cells at the free surface have at least one

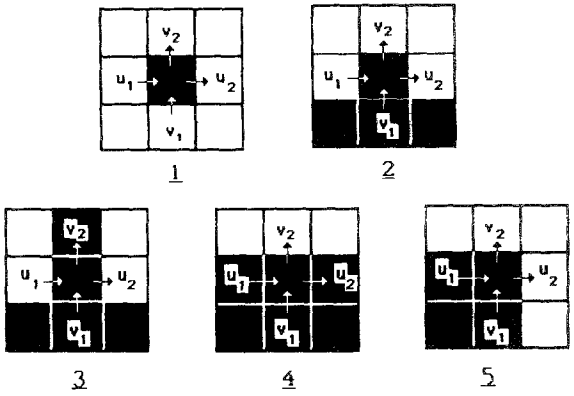

FIG. 12. Possible cases of surface cell relations with neighboring cells in momentum calculations.

cell boundary-facing vacuum. This makes the evaluation of the neighboring velocities in that direction impossible. Based on the marker and cell method [12], the continuity equation is to be used for the surface cells to calculate the velocity at the free surface. For a wet cell without any wet neighboring cells (i.e., case 1) there is no way that the velocity of the cell will be changed. As a matter of fact, a wet cell without wet neighbors is considered a different computational domain from the major body of the fluid. Therefore, it is thrown away in the following computation. For a wet cell with wet neighboring cells except one face, the velocity component at that free surface is obtained by equating it to the required value obtained

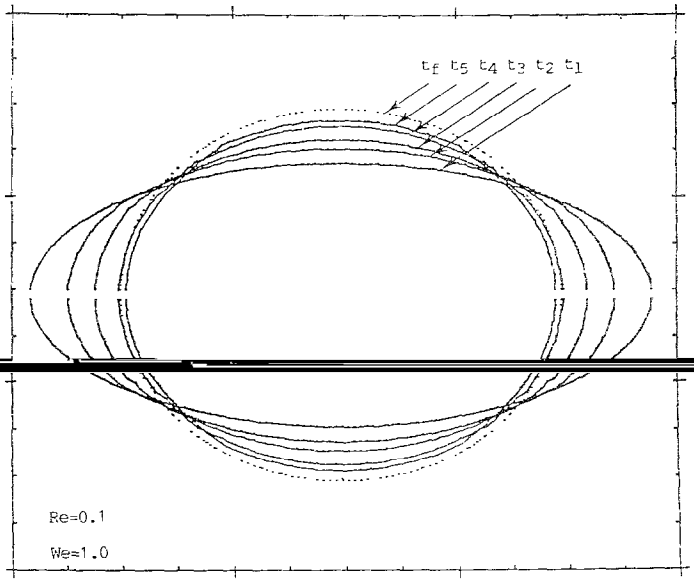

FIG. 13. Damping oscillation of an originally elliptic infinite cylinder.

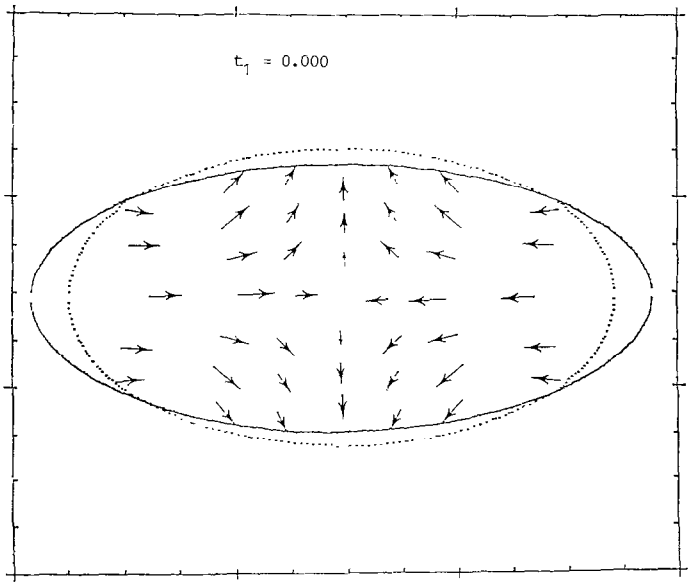

(a)

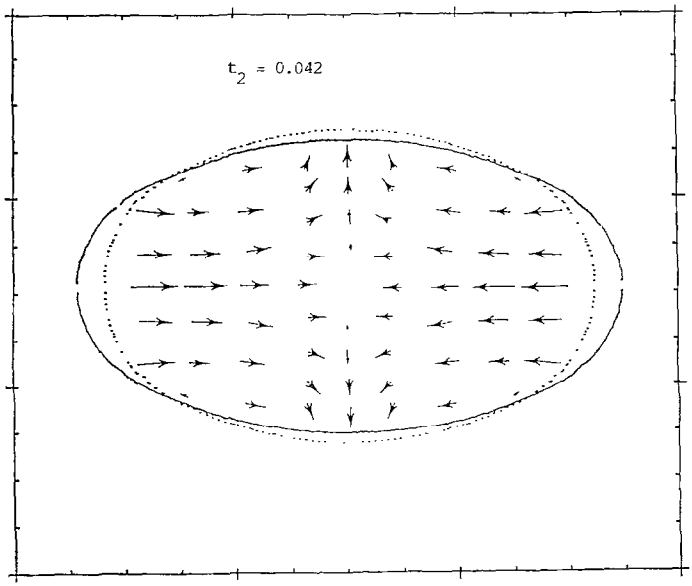

(b)

FIG. 14. Internal velocity field and shape of the drop at different times.

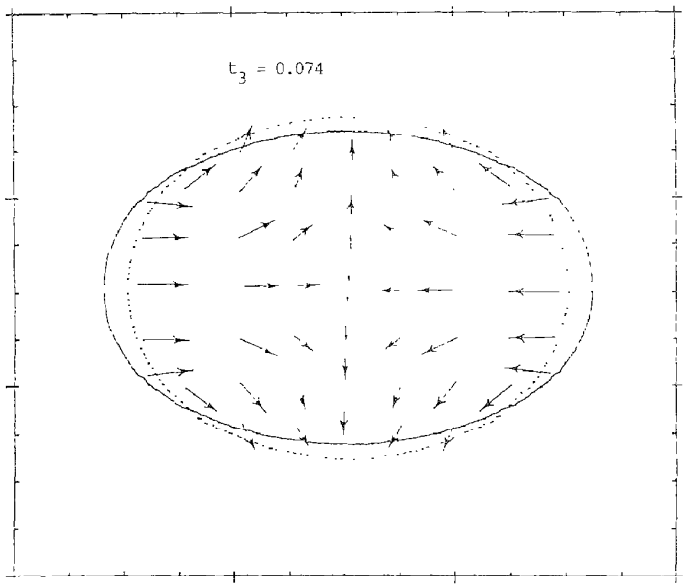

(c)

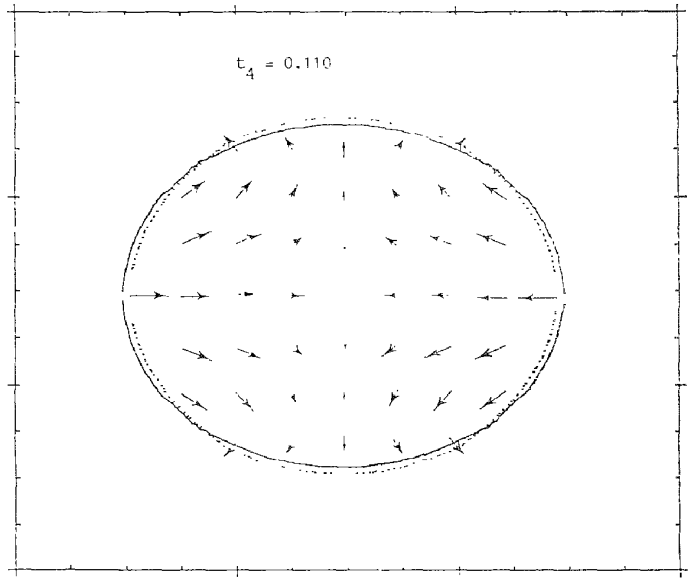

(d)

FIG. 14—*Continued*

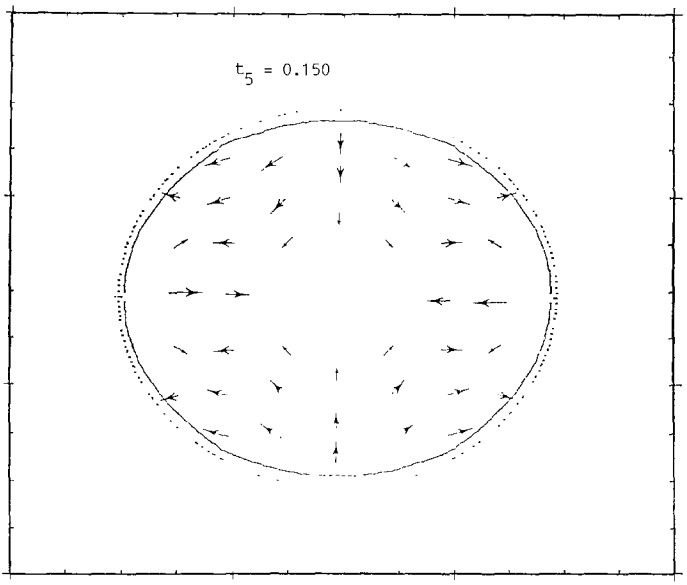

(e)

FIG. 14—*Continued*

from the continuity equation. For example, in case 2, $v_2 = v_1 + u_1 - u_2$. For a wet cell with two dry faces, the velocity component at the free surface is equated to the velocity component in the opposite side. For example, in case 3, $u_2 = u_1$ and $v_2 = v_1$. For a wet cell with three dry faces, the velocity component at the free surface opposite to the wet side is set equal to that of the wet side. For the velocity component at the two opposing dry faces, the two velocities are assumed to retain their values. For example, in case 4, $v_2 = v_1$ and $u_2 = u_1 = u_{1p}$ (subscript p refers to the value at the previous time step).

Using the momentum equations for the interior cells and continuity equations for the surface cells, a set of equations relating pressure and velocities for all the cells can be set up. These equations can be solved using the boundary conditions. The only boundary condition in this problem is the pressure at the free surface. This pressure is obtained by the calculation of the surface curvature. The surface curvature is obtained by using the technique developed by Poo and Ashgriz [27]. Very briefly, this method uses a second-order polynomial, based on the area fraction field at the surface, to represent the local surface equation. Once the equation describing the surface is known, the surface curvature at each cell can be determined.

Based on the above discussions, the solution procedure can be summarized as follows: (1) Specify the initial conditions for the surface geometry and velocities. (2) Move the surface based on these velocities and the FLAIR algorithm. (3) Find the surface curvature based on the cell volume fractions. (4) Calculate the surface pressure based on the local values of surface curvatures and Eq. (27). (5) Calculate

the pressure throughout the drop using Poisson's equation. (6) Solve for the velocity field throughout the drop using the momentum equations. (7) Iterate between steps (6) and (7) until convergence is achieved. (8) Increment the time and repeat.

The results for the motion of an initially elliptic drop are presented in Figs. 13 and 14. Initially, the major diameter of the ellipse is set equal to 1, and its minor diameter to 0.5, with mesh size of 0.01 and zero velocities everywhere. However, because of the non-uniform curvature on the surface of the ellipse, there will be a capillary driven flow. This flow will eventually damp out and the equilibrium condition of stationary circular drop will be attained. The damping motion of the drop is shown in Fig. 13. The Reynolds number used for this case is 0.1, and the Weber number is 1.0. The Weber number is defined based on the initial major diameter of the ellipse, D. Because the drop's initial velocity is zero, the velocity scale is obtained by setting the Weber number equal to 1 and then calculating the velocity scale from $u = \sqrt{\sigma/\rho D}$. Figure 13 shows the drop shape at different times. It is observed that, due to high viscosity, the drop shape becomes circular within a few oscillations. Figures 14a–e show the velocity field inside the drop at different times. The oscillation of the drop generates a recirculation zone within it, which also damps out after the drop ceases motion. The smoothness of the surface after long computational times indicates the accuracy of this technique for surface movement and therefore it has better curvature calculations. It is noteworthy that there exists an area loss in the computations because the actual shape of a surface cell is not used in the continuity equation. However, as other VOF techniques do, one can distribute the loss in volume fraction during the surface advection and reconstruction among the cells, such that the total area loss remains zero. However, in the present calculation we are more concerned with the presentation of the technique; therefore, no corrections of that sort are made.

Conclusions

A new technique of interface transport and reconstruction is developed for the numerical models using the volume of fluid (VOF) method. The basic features of this technique are as follows: The interface is assumed to be represented by a set of line segments fitted at the boundary of every two neighboring surface cells. A criterion is developed which identifies the orientation of the line segment based only on the volume fractions of the two cells. This criterion is developed based on realizing that there can be only a limited number of cases for arrangement of two neighboring cells. After the surface orientation is determined, the volume fraction field is updated by calculating the fluid flux across any two neighboring cells. It is shown that the flux line segment model for advection and interface reconstruction (FLAIR) technique is more accurate in advection of the fraction of volume field than the more common donor–acceptor technique.

REFERENCES

1. R. W. YEUNG, *Annu. Rev. Fluid Mech.* **14**, 395 (1982).
2. A. S. GELLER, S. H. LEE, AND L. G. LEAL, *J. Fluid Mech.* **169**, 27 (1986).
3. J. M. RALLISON AND A. ACRIVOS, *J. Fluid Mech.* **89**, 191 (1978).
4. R. BONNEROT AND P. JAMET, *J. Comput. Phys.* **25**, 163 (1977).
5. D. R. LYNCH, *J. Comput. Phys.* **47**, 387 (1982).
6. P. BACH AND O. HASSAGER, *J. Fluid Mech.* **152**, 173 (1985).
7. I. S. KANG AND L. G. LEAL, *Phys. Fluids* **30**, 1929 (1987).
8. G. RYSKIN AND L. G. LEAL, *J. Fluid Mech.* **148**, 1 (1984).
9. N. S. ASAITHAMBI, *J. Comput. Phys.* **73**, 380 (1987).
10. D. E. FYFE, E. S. ORAN, AND M. J. FRITTS, Naval Res. Lab. NRL Memorandum Report No. 6185, 1988 (unpublished).
11. M. J. FRITTS AND J. P. BORIS, *J. Comput. Phys.* **31**, 173 (1979).
12. J. E. WELCH, F. H. HARLOW, J. P. SHANNON, AND B. J. DALY, Los Alamos Scientific Lab. Report No. LA-3425, 1966 (unpublished).
13. F. H. HARLOW AND J. F. WELCH, *Phys. Fluids* **8**, 2182 (1965).
14. H. MIYATA AND S. NISHIMURA, *J. Fluid Mech.* **157**, 327 (1985).
15. H. MIYATA, *J. Comput. Phys.* **65**, 179 (1986).
16. C. W. HIRT AND B. D. NICHOLS, *J. Comput. Phys.* **39**, 201 (1981).
17. B. D. NICHOLS, C. W. HIRT, AND R. S. HOTCHKISS, Los Alamos Scientific Lab. Report No. LA8355, 1980 (unpublished).
18. M. D. TORREY, L. D. CLOUTMAN, R. C. MJOLSNESS, AND C. W. HIRT, Los Alamos National Lab. Report No. LA-10612-MS, 1985 (unpublished).
19. W. F. NOH, "CEL: A Time Dependent, Two Space Dimensional, Coupled Eulerian Lagrange Code," in *Methods in Computational Physics, Vol. 3*, edited by B. Adler, S. Fernbach, and M. Rotenberg (Academic Press, New York/London, 1964), p. 117.
20. W. F. NOH AND P. WOODWARD, in *Proceedings of the Fifth International Conference on Numerical Methods in Fluid Dynamics*, edited by A. I. van de Vooren and P. J. Zandbergen, Lecture Notes in Physics, Vol. 59 (Springer-Verlag, New York, 1976), p. 330.
21. P. K. BARR AND W. T. ASHURST, Sandia National Lab. Report No. SAND82-8773, 1984 (unpublished).
22. A. J. CHORIN, *J. Comput. Phys.* **35**, 1 (1980).
23. A. J. CHORIN, *J. Comput. Phys.* **57**, 472 (1985).
24. J. A. SETHIAN, *Commun. Math. Phys.* **101**, 487 (1985).
25. R. B. DEBAR, Lawrence Livermore Lab. Report No. UCID-17366, 1974 (unpublished).
26. D. L. YOUNGS, "Time-Dependent Multi-Material Flow with Large Fluid Distortion," in *Numerical Methods for Fluid Dynamics*, edited by K. W. Morton and M. J. Baines (Academic Press, New York, 1982), p. 27.
27. J. Y. POO AND N. ASHGRIZ, *J. Comput. Phys.* **84**, 483 (1989).